

ShapePuri: Shape Guided and Appearance Generalized Adversarial Purification

Zhe Li, Bernhard Kainz
 Department AIBE, FAU Erlangen-Nürnberg, Germany
 zhe.li@fau.de

Abstract

Deep neural networks demonstrate impressive performance in visual recognition, but they remain vulnerable to adversarial attacks that are imperceptible to the human. Although existing defense strategies such as adversarial training and purification have achieved progress, diffusion-based purification often involves high computational costs and information loss. To address these challenges, we introduce Shape Guided Purification (ShapePuri), a novel defense framework enhances robustness by aligning model representations with stable structural invariants. ShapePuri integrates two components: a Shape Encoding Module (SEM) that provides dense geometric guidance through Signed Distance Functions (SDF), and a Global Appearance Debiasing (GAD) module that mitigates appearance bias via stochastic transformations. In our experiments, ShapePuri achieves 84.06% clean accuracy and 81.64% robust accuracy under the AutoAttack protocol, representing the first defense framework to surpass the 80% threshold on this benchmark. Our approach provides a scalable and efficient adversarial defense that preserves prediction stability during inference without requiring auxiliary modules or additional computational cost.

1. Introduction

Modern vision models have achieved unprecedented success in complex visual tasks, but their inherent vulnerability to adversarial perturbations reveals a fundamental discrepancy between human perception and neural representations. A subtle and imperceptible noise can catastrophically degrade model reliability, posing significant risks to safety-critical deployments such as autonomous driving and biometric security. This sensitivity to minor input variations undermines the practical reliability of automated systems in diverse operational scenarios. Consequently, developing reliable and efficient defense strategy remains a pivotal challenge AI security.

The defense against adversarial attacks has primarily bifurcated into two paradigms: adversarial training (AT) and

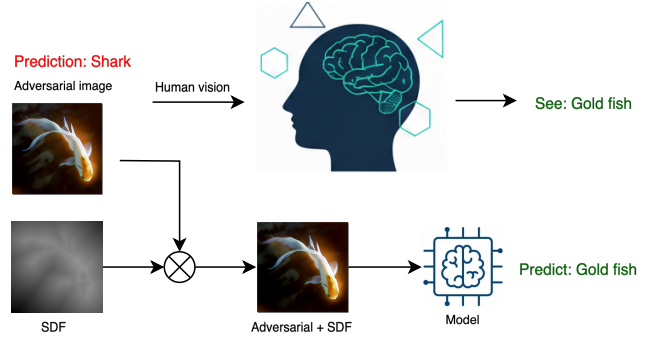


Figure 1. Our method utilizes Signed Distance Functions (SDF) to enrich adversarial images, aligning model predictions with human perception to defense adversarial attack.

adversarial purification. AT methods directly regularize the model parameters against specific attack budgets but often suffer from a trade-off between robustness and accuracy and limited generalization to unseen or adaptive threats. Conversely, adversarial purification treats robustness as an inference-time preprocessing task, aiming to project adversarial inputs back onto the clean image manifold. Recently, diffusion-based models [11, 15, 22] have emerged as the dominant framework for purification, utilizing iterative denoising to eliminate perturbations. Despite their empirical success, diffusion-based methods encounter two fundamental bottlenecks: (1) High computational cost, where the multi-step reverse sampling process introduces significant latency for real time applications; and (2) Fidelity degradation, where the generative nature of diffusion models tends to prioritize distribution matching over exact reconstruction, often hallucinating textures and losing instance-specific details critical for fine-grained classification.

In this work, we propose a shift from the generative denoising paradigm toward a structure-aware purification framework. This transition arises from the observation that human vision exhibits a robust shape preference, maintaining semantic consistency across variations in illumination, texture, and noise (Fig. 1). In contrast, standard DNNs are predominantly biased toward local textures and

high-frequency appearance features, precisely the components most susceptible to adversarial manipulation. Crucially, while adversarial perturbations significantly alter pixel-level intensities, they typically leave the underlying geometric skeleton and global structure of the object intact. We therefore hypothesize that a purification mechanism that explicitly reinforces geometric invariance while marginalizing fragile appearance features can yield superior robustness without the stochastic overhead of diffusion.

Building upon this intuition, we introduce Shape-Guided Purification (ShapePuri), a deterministic and lightweight defense framework that emphasizes shape-centric representations through two synergistic components. Specifically, we first propose the Shape Encoding Module (SEM), which provides an explicit geometric anchor by augmenting the input with its Signed Distance Field (SDF). As a continuous, low-frequency spatial representation of object boundaries derived from global topology, the SDF remains remarkably stable under local pixel perturbations, guiding the classifier to prioritize invariant geometric cues over perturbed appearance. Complementing this, we introduce Global Appearance De-biasing (GAD), which adapts the concept of global intensity transformations to mitigate the model inherent appearance bias. By leveraging non-linear convolutional transformations, GAD marginalizes spurious appearance dependent features, thereby breaking the reliance on fragile textural shortcuts exploited by adversarial attacks. This de-biasing process recenters the model perception on stable geometric structures while maintaining the representational integrity necessary for accurate recognition.

ShapePuri provides a robust alternative to iterative generative reconstruction, offering a more reliable and efficient defense. Extensive evaluations on ImageNet demonstrate that ShapePuri achieves an unprecedented 81.64% robust accuracy under the rigorous AutoAttack benchmark, outperforming the previous diffusion-based state-of-the-art (SOTA) by a significant margin of 7.45%. To the best of our knowledge, this is the first defense framework to surpass the 80% robust accuracy threshold on ImageNet.

Our main contributions are as follows:

1. We propose ShapePuri, a novel diffusion-free adversarial purification framework that anchors visual perception in invariant geometric structures. By leveraging these shape-oriented representations, ShapePuri ensures robust defense against appearance perturbations.
2. We introduce a dual-component architecture consisting of a Shape Encoding Module (SEM) for continuous geometric stabilization and Global Appearance De-biasing (GAD) for effective appearance de-biasing.
3. Our framework establishes a new state-of-the-art on ImageNet, achieving 81.64% robust accuracy under AutoAttack while maintaining high clean accuracy and zero computation cost at inference compared to generative

models.

2. Related work

Adversarial training. Madry *et al.* [14] formulate adversarial robustness as a min–max optimization problem and propose the Projected Gradient Descent (PGD) attack as a principled first-order adversary. Subsequently, AutoAttack [4] introduces an ensemble of parameter-free attacks to provide more reliable evaluations. Recent research has investigated diverse adversarial defense strategies by focusing on data augmentation with synthetic samples [6] and architectural refinements like the ConvStem in vision transformers [21]. Furthermore, techniques such as MeanSparse [1] leverage post training feature sparsification, while IJSAT [10] utilizes normalizing flows to model the data manifold. These methods primarily enhance robustness through direct optimization or structural modification of the classifier.

Adversarial purification. Early purification strategies employed generative models, such as Defense GAN [19] or Variational Autoencoder (VAE) ensembles [20], to project perturbed inputs onto the clean data manifold. However, these methods often struggle with scalability and adaptive adversaries. Recently, diffusion-based denoising has emerged as a dominant paradigm. DiffPure [15] utilizes forward and reverse diffusion, while GDMP [22] and Bai *et al.* [2] introduce guided reverse processes to stabilize semantic recovery. Despite their efficacy, the multi-step sampling required by diffusion models introduces substantial computational costs. While OSCP [11] attempts to reduce this overhead through distillation, the underlying diffusion process remains prone to information loss.

Structural guidance and appearance debiasing. Existing research utilizes edge maps as an auxiliary guide for diffusion based models [11]. However, this edge representation is inherently sparse and lacks informative gradients across the image domain, which restricts the efficacy of semantic recovery. The utilization of dense structural priors thus remains largely unexplored in adversarial purification. To address these limitations, we leverage SDF to provide a continuous spatial field representation of geometry. The capacity of SDF is already proven in 3D surface reconstruction [18] and robust outlier detection [3]. Our framework is the first effort to internalize these continuous spatial fields as a primary purification mechanism. Detailed investigations [5] reveal that standard models rely heavily on local texture rather than global object shape, which contrasts with the structural focus characterizing human perception. This reliance on non robust features constitutes a primary source of adversarial vulnerability [8]. To mitigate this, appearance debiasing through stochastic transformations encourages the internalization of semantic invariants [9]. Our GAD module adopts this principle by using randomized shallow convolutions [17] to foster appearance in-

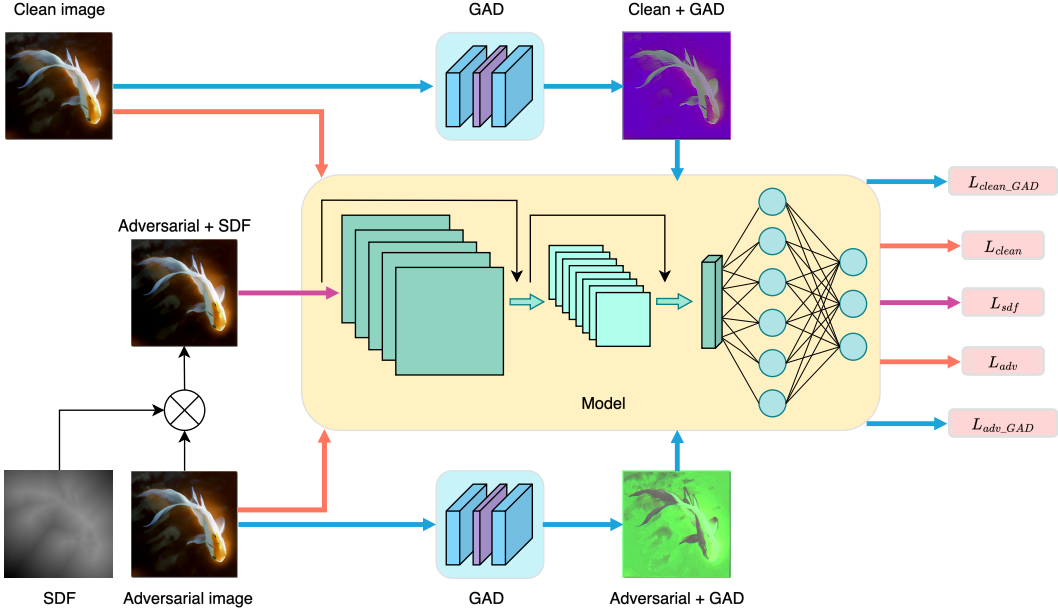


Figure 2. Overview of the proposed Shape-Guided Purification framework. For each clean image, the input consists of five distinct variants processed through different streams. In the top branch, the framework processes clean images via two paths: a direct input to the backbone (orange line) and an input refined through the Global Appearance De-biasing (GAD) module (blue line). The bottom branch mirrors this structure for adversarial images, utilizing both direct and GAD processed versions (orange and blue lines). In the middle stream, adversarial images are fused with Signed Distance Functions (SDF) to enhance structural consistency. The model is supervised by five distinct loss functions, including L_{clean_GAD} , L_{clean} , L_{sdf} , L_{adv} , and L_{adv_GAD} , each corresponding to a specific input variant to ensure robust feature representation and successful purification.

variance while preserving underlying semantics.

3. Method

ShapePuri is a unified training framework designed to enhance adversarial robustness by prioritizing stable shape structures over unreliable appearance features. Our core philosophy is to integrate shape-driven guidance directly into the training phase, enabling the model to internalize purified representations that are inherently resilient to perturbations. Given a clean image I and its adversarial counterpart $I_{adv} = I + \delta$ (where $\|\delta\|_p \leq \epsilon$), we optimize the model parameters θ such that the classifier f_θ maintains consistent predictions, i.e., $f_\theta(I_{adv}) \approx f_\theta(I)$, by focusing on structural invariants.

As illustrated in Fig. 2, ShapePuri leverages five parallel input streams throughout the training phase to provide diverse learning cues. Specifically, a Shape Encoding Module (SEM) incorporates Signed Distance Functions (SDF) to reinforce geometric awareness, while a Global Appearance De-biasing (GAD) module mitigates over-reliance on non-robust textures. These paths are optimized via a joint training objective, allowing the model to internalize robust information. Crucially, during inference, the model operates as a standard classifier without these auxiliary mod-

ules and additional computational cost. We first establish the SDF-based shape encoding in Sections 3.1 and 3.2, followed by the descriptions of the GAD module in Section 3.3 and the integrated training objective in Section 3.4.

3.1. Preliminaries

An SDF is a scalar function that encodes the distance from any point in space to a closed surface, with the sign indicating whether the point lies inside or outside the surface. Following the classical formulation in level-set methods [16], we define the SDF as:

$$\phi(\mathbf{x}) = \begin{cases} + \min_{\mathbf{y} \in \partial\Omega} \|I - \mathbf{y}\|, & I \in \Omega \quad (\text{inside}) \\ 0, & I \in \partial\Omega \quad (\text{on surface}) \\ - \min_{\mathbf{y} \in \partial\Omega} \|I - \mathbf{y}\|, & I \in \mathbb{R}^n \setminus \Omega \quad (\text{outside}), \end{cases} \quad (1)$$

where $\Omega \subset \mathbb{R}^n$ is a closed domain, $\partial\Omega$ denotes its boundary, and $\|\cdot\|$ is the Euclidean norm. By construction, the zero level set of $\phi(I)$ implicitly defines the surface, the gradient $\nabla\phi(I)$ points outward along the surface normal, and $|\phi(I)|$ gives the exact distance to the surface.

The SDF provides a continuous and differentiable representation of geometry, which is particularly advantageous for gradient-based optimization, collision detection, level

set methods, and rendering. Its key properties are as follows. First, the magnitude $|\phi(I)|$ represents the exact Euclidean distance to the nearest surface. Second, the gradient $\nabla\phi(I)$ is a normalized vector pointing outward from the object interior, *i.e.*, $\|\nabla\phi(I)\| = 1$ almost everywhere. The zero level set ($\phi(I) = 0$) implicitly defines the surface geometry, enabling operations such as Boolean combinations, surface smoothing, and volumetric manipulations.

3.2. Shape encoding module

To incorporate robust geometric priors, we introduce the Shape Encoding Module (SEM), which anchors the purification process in global geometric structures to mitigate the impact of pixel-level adversarial noise. We employ the Signed Distance Function (SDF) to transform discrete image masks into continuous spatial fields, where each pixel value represents the shortest Euclidean distance to the nearest object boundary. This dense representation provides a structural complement to pixel-level appearance features, facilitating a geometry-aware learning process.

SDF construction. Given an input image I (Fig. 3 (a)), we first apply Gaussian smoothing to suppress high-frequency noise (Fig. 3 (b)) to facilitate stable boundary extraction. An adaptive Otsu thresholding is then utilized to generate a binary mask I_{mask} (Fig. 3 (c)), where foreground pixels are assigned to 1 and background pixels to 0. Based on this mask, we compute the final SDF (Fig. 3 (f)) by calculating the difference between the inner and outer Euclidean distance transforms:

$$\text{inner} = \text{DT}(I_{\text{mask}}), \text{outer} = \text{DT}(1 - I_{\text{mask}}) \quad (2)$$

$$I_{\text{SDF}} = \text{inner} - \text{outer} \quad (3)$$

where $\text{DT}(\cdot)$ denotes the Euclidean distance transform. The inner transform (Fig. 3 (d)) measures the minimum distance from object interior pixels to the boundary, while the outer transform (Fig. 3 (e)) encodes the distance for background pixels. Because object regions are typically compact relative to the background, the inner distances remain bounded within a small range whereas the outer distances can attain significantly larger magnitudes, leading to distinct statistical distributions for foreground and background regions even though both fields exhibit similar local gradient behavior near the boundary. This statistical divergence ensures a clear differentiation of regions across the image domain, resulting in a continuous spatial field that effectively encodes global shape information. Beyond single-object representation, this pixel-wise encoding naturally accommodates the geometry of multiple objects simultaneously to provide a holistic structural prior.

Foreground consistency refinement. To ensure the reliability of the geometric prior, we introduce a multi-stage

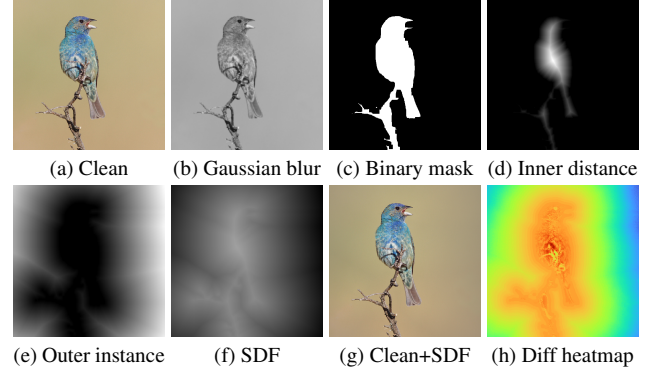


Figure 3. Illustration of the SDF computation steps.

refinement pipeline to correct potential errors in the initial binary mask, such as sign inversion typically caused by dark objects appearing on light backgrounds or fragmented segments. We first verify the foreground assignment using mean pixel intensity $\mu = \frac{1}{HW} \sum_{i,j} I_{\text{mask}}(i,j)$. Specifically, we leverage the statistical prior that background regions typically dominate the image area to mitigate sign ambiguity. If $\mu > \tau$ (where $\tau \in [0, 1]$ is a predefined threshold), the mask is inverted to ensure the object is correctly encoded as foreground. This prior is empirically valid for the vast majority of natural samples. Even in rare cases of prior failure (e.g., extreme close-ups), the resulting mask remains resilient as it still provides a contrastive signal that aids robust feature learning. Following this, connected components $\{C_k\}_{k=1}^K$ are identified, and the principal object C^* is selected by maximizing a geometric score:

$$C^* = \arg \max_{C_k} S_k, \quad S_k = A_k \bar{D}_k^2 \quad (4)$$

where $A_k = |C_k|$ denotes the pixel area and \bar{D}_k is the mean foreground distance transform. To preserve structural continuity, neighboring components within a small Euclidean margin δ from ∂C^* are merged into C^* . Finally, a flood-fill operation is performed from the image boundary to ensure topological consistency, yielding a hole-free and continuous object region. The refined mask I_{mask} thus obtained serves as the finalized input for subsequent SDF computation.

Shape-guided image fusion. The normalized SDF (Fig. 3 (f)) is integrated with the adversarial image to form an enhanced representation (Fig. 3 (g)) that highlights structural salience. The fusion is defined as:

$$I_{\text{fusion}} = I_{\text{adv}} \odot (1 + \beta I_{\text{SDF}}), \quad (5)$$

where \odot denotes element-wise multiplication and $\beta \in \mathbb{R}^+$ controls the strength of geometric modulation. This spatial modulation adaptively amplifies object interior intensities while attenuating background regions, thereby reinforcing

Algorithm 1 ShapePuri Training Procedure

Notation:

f_θ : Trainable classifier with parameters θ .

$\mathcal{A}(\cdot)$: Adversarial attack operator.

$\mathcal{S}(\cdot)$: SDF computation.

$g_\theta(\cdot)$: GAD transformation.

- 1: **Input:** Dataset \mathcal{D} , Hyperparameter β .
- 2: **for** each step **do**
- 3: Sample mini-batch $(I_B, y_B) \sim \mathcal{D}$
- 4: Generate adversarial samples: $I_{\text{adv}} \leftarrow \mathcal{A}(I)$
- 5: $L_{\text{base}} = \mathcal{L}_{\text{CE}}(f_\theta(I_B), y) + \mathcal{L}_{\text{CE}}(f_\theta(I_{\text{adv}}), y)$
- 6: $I_{\text{SDF}} \leftarrow \mathcal{S}(I)$
- 7: $I_{\text{fusion}} = I_{\text{adv}} \odot (1 + \beta \cdot I_{\text{SDF}})$
- 8: $L_{\text{SDF}} = \mathcal{L}_{\text{CE}}(f_\theta(I_{\text{fusion}}), y)$
- 9: $I_{\text{GAD}} \leftarrow g_\theta(I_B); I_{\text{adv}}^{\text{GAD}} \leftarrow g_\theta(I_{\text{adv}})$
- 10: $L_{\text{GAD}} = \mathcal{L}_{\text{CE}}(f_\theta(I_{\text{GAD}}), y) + \mathcal{L}_{\text{CE}}(f_\theta(I_{\text{adv}}^{\text{GAD}}), y)$
- 11: $L_{\text{total}} = L_{\text{base}} + L_{\text{SDF}} + L_{\text{GAD}}$
- 12: Update f_θ via backpropagation
- 13: **end for**

ing boundary contrast and guiding the model toward robust structural invariants. The structural integrity after fusion is further validated via a pixel-wise difference heatmap Fig. 3 (h), which confirms that the geometric cues are effectively injected without distorting the global appearance.

3.3. Global Appearance De-biasing

The Global Appearance De-biasing (GAD) module is designed to address the inherent sensitivity of neural networks to appearance cues, which frequently serve as vulnerable proxies exploited by adversarial perturbations. GAD applies stochastic transformations to local intensity and texture, thereby increasing the diversity of visual representations. In practice, the module modulates the visual characteristics of the input to prevent over-reliance on non-robust patterns rather than suppressing appearance information altogether. This integrated strategy effectively steers the model toward robust geometric invariants that remain consistent across diverse appearance variations.

During training, both clean and adversarial images are processed through GAD before being passed to the classifier. The core of this module consists of a family of shallow, two-layer stochastic convolutional networks $g(\cdot) \in \mathcal{G}$ that perform localized transformations while preserving spatial relationships. Each instantiation within this family effectively defines a stochastic operator that takes an input image $I \in \mathbb{R}^{C \times H \times W}$ and generates a transformed output: $g(\cdot) : \mathbb{R}^{C \times H \times W} \rightarrow \mathbb{R}^{C \times H \times W}$, where C is the number of channels and H, W are the spatial dimensions.

At each iteration, new convolutional parameters are sampled from a Gaussian distribution $\mathcal{N}(0, 1)$. We employ small receptive fields to restrict the transformation to local

texture variations, while Leaky ReLU activations introduce the non-linearity necessary for diverse appearance modeling. The modulated output is obtained by linearly interpolating the original image I with the stochastic network output $g_\theta^{\text{Net}}(I)$, using an interpolation coefficient α sampled from a uniform distribution $\mathcal{U}(0, 1)$. To ensure that the debiasing process does not introduce global artifacts or shift the mean luminance, we re-normalize the transformed image to match the Frobenius norm [17] of the original input I . The finalized transformation is expressed as:

$$g_\theta(I) = \frac{\alpha g_\theta^{\text{Net}}(I) + (1 - \alpha)I}{\|\alpha g_\theta^{\text{Net}}(I) + (1 - \alpha)I\|_F} \cdot \|I\|_F, \quad (6)$$

where $\|\cdot\|_F$ denotes the Frobenius norm. GAD is computationally efficient due to its shallow design and is fully differentiable, enabling its seamless integration into various adversarial training and purification frameworks.

3.4. Training objective

The framework is trained end-to-end using a multi-stream supervision strategy involving five distinct input variations that encapsulate the proposed structural and appearance priors. Given a batch of clean samples (I_B, y_B) and their adversarial counterparts I_{adv} , the base classification loss is defined as: $L_{\text{base}} = \mathcal{L}_{\text{CE}}(f_\theta(I), y) + \mathcal{L}_{\text{CE}}(f_\theta(I_{\text{adv}}), y)$, where f_θ denotes the classifier and $\mathcal{L}_{\text{CE}}(\cdot)$ denotes the cross entropy loss. To explicitly reinforce object structural integrity, we incorporate a geometry guided loss term L_{SDF} using the shape enhanced adversarial image $I_{\text{adv_SDF}}$.

$$L_{\text{SDF}} = \mathcal{L}_{\text{CE}}(f_\theta(I_{\text{adv_SDF}}), y) \quad (7)$$

$$L_{\text{GAD}} = \mathcal{L}_{\text{CE}}(f_\theta(g_\theta(I_B)), y) + \mathcal{L}_{\text{CE}}(f_\theta(g_\theta(I_{\text{adv}})), y) \quad (8)$$

$$L_{\text{total}} = L_{\text{base}} + L_{\text{SDF}} + L_{\text{GAD}} \quad (9)$$

Further, the appearance debiasing objective L_{GAD} is calculated to identify semantic invariants from adversarial perturbations. The total training objective is the summation of the base, geometric, and appearance losses. The overall algorithm is summarized in Algorithm 1.

4. Experiments

4.1. Implementation details

Training setup. We split the ImageNet validation set into 40,000 images for training and 10,000 for testing, following OSCP [11] to ensure consistent comparison with prior work. All images are resized to a resolution of 512×512 . We train and evaluate our framework on ResNet-101 under untargeted PGD-100 attacks, ResNet-152 under targeted PGD-40 attacks, and ConvNeXt-L under AutoAttack. Each classifier is initialized with ImageNet-pretrained weights.

Table 1. Comparison with state-of-the-art. Accuracy (%) results for ImageNet.

Attacks	Defense	Clean Accuracy	Robust Accuracy	Classifiers	Domain
untargeted PGD-100	Without defense	80.55	0.01	ResNet-50	Without defense
	GDMP [22]	73.53	72.97	ResNet-50	Adversarial Purification
	OSCP [11]	77.63	73.89	ResNet-50	Hybrid
	ShapePuri (ours)	79.47	76.43	ResNet-101	Hybrid
targeted PGD-40	Without defense	82.33	0.04	ResNet-152	Without defense
	GDMP [22]	78.10	77.86	ResNet-152	Adversarial Purification
	OSCP [11]	79.81	78.78	ResNet-152	Hybrid
	ShapePuri (ours)	80.73	79.02	ResNet-152	Hybrid
AutoAttack	Without defense	80.55	0.00	ResNet-50	Without defense
	MeanSparse [1]	77.96	59.64	ConvNeXt-L	Adversarial Training
	Singh <i>et al.</i> [21]	77.00	57.70	ConvNeXt-L	Adversarial Training
	DiffPure [15]	75.77	73.02	ResNet-50	Adversarial Purification
	OSCP [11]	77.63	74.19	ResNet-50	Hybrid
	ShapePuri (ours)	84.06	81.64	ConvNeXt-L	Hybrid

The initial learning rate is set to 1×10^{-4} and decayed using a StepLR scheduler with period 2500 and decay factor 0.5. The range of shape pixel value is $[-1, +1]$ and the shape control parameter β is fixed at 0.5 in all experiments. We report clean accuracy, defined as performance on unper- turbed inputs, and robust accuracy, defined as performance on adversarially perturbed inputs.

Attack setup. We adopt the same attack families for training and evaluation to ensure consistency. Adversarial samples are generated using PGD [14] and AutoAttack [4] under L_p constraints. We use ϵ to denote the L_∞ perturbation bound, the maximum allowed per pixel change. PGD-n denotes a PGD attack with n iterations. For untargeted PGD-100, we set $\epsilon = 4/255$, step size $\eta = 1/255$, and 100 iterations. For targeted PGD-40, we set $\epsilon = 16/255$, step size $\eta = 0.4/255$, and 40 iterations. For AutoAttack, we use the standard ensemble consisting of four attacks applied in the following order: APGD with cross entropy loss, APGD with DLR loss, FAB, and Square, with $\epsilon = 4/255$. In all experiments, the attack models are same to the training models. The attacks are heavier if the models are larger.

4.2. Comparison with state-of-the-art

The efficacy of ShapePuri is validated through a comprehensive evaluation compared to current state-of-the-art defense mechanisms, as summarized in Tab. 1. The results indicate that ShapePuri consistently delivers superior clean and robust accuracy across diverse adversarial settings. Under the untargeted PGD-100 attack, ShapePuri reaches 79.47% clean accuracy and 76.43% robust accuracy, surpassing the diffusion-based defense OSCP [11] by 1.8% and 2.54%, respectively. In the targeted PGD-40 attack,

ShapePuri slightly improves the performance to 80.73% clean and 79.02% robust accuracy. For the strong AutoAt- tack, ShapePuri yields substantial gains and improves clean accuracy by 6.1% (84.06% vs. 77.96%) and robust accuracy by 7.45% (81.64% vs. 74.19%). Notably, ShapePuri is the first defense framework to exceed 80% robust accuracy threshold. Furthermore, we conduct a fine grained analysis on category specific subsets of ImageNet. The frame- work achieves 82.56% average accuracy across 125 dog classes and 94.92% across 59 bird classes. This demon- strate that ShapePuri mitigates the adversarial sensitivity to non-robust textures while maintaining the discriminative fidelity required for precise classification. Qualitative results shown in Fig. 4 illustrate the capability of the model to pre- serve semantic structure and boundary integrity even under adversarial perturbations.

4.3. Ablation study

Effect of SEM and GAD modules We investigate the individual contributions of the SEM and GAD modules by evaluating their performance in isolation. The results in Tab. 2 indicate that each module independently enhances adversarial resilience. In the untargeted setting, the combination reflects a synergistic balance between the GIR-only and SDF- only settings. SDF alone improves the robust accuracy to 77.11, and GAD enhances the clean accuracy to 79.47, confirming that these components are complementary. The advantage of integrating both modules becomes most evident under the stronger AutoAttack benchmark. GIR improves clean accuracy (82.20% to 84.06%) and robust accuracy (80.30% to 81.64%) over the SDF-only baseline. These findings demonstrate that GAD acts as a structural regular-

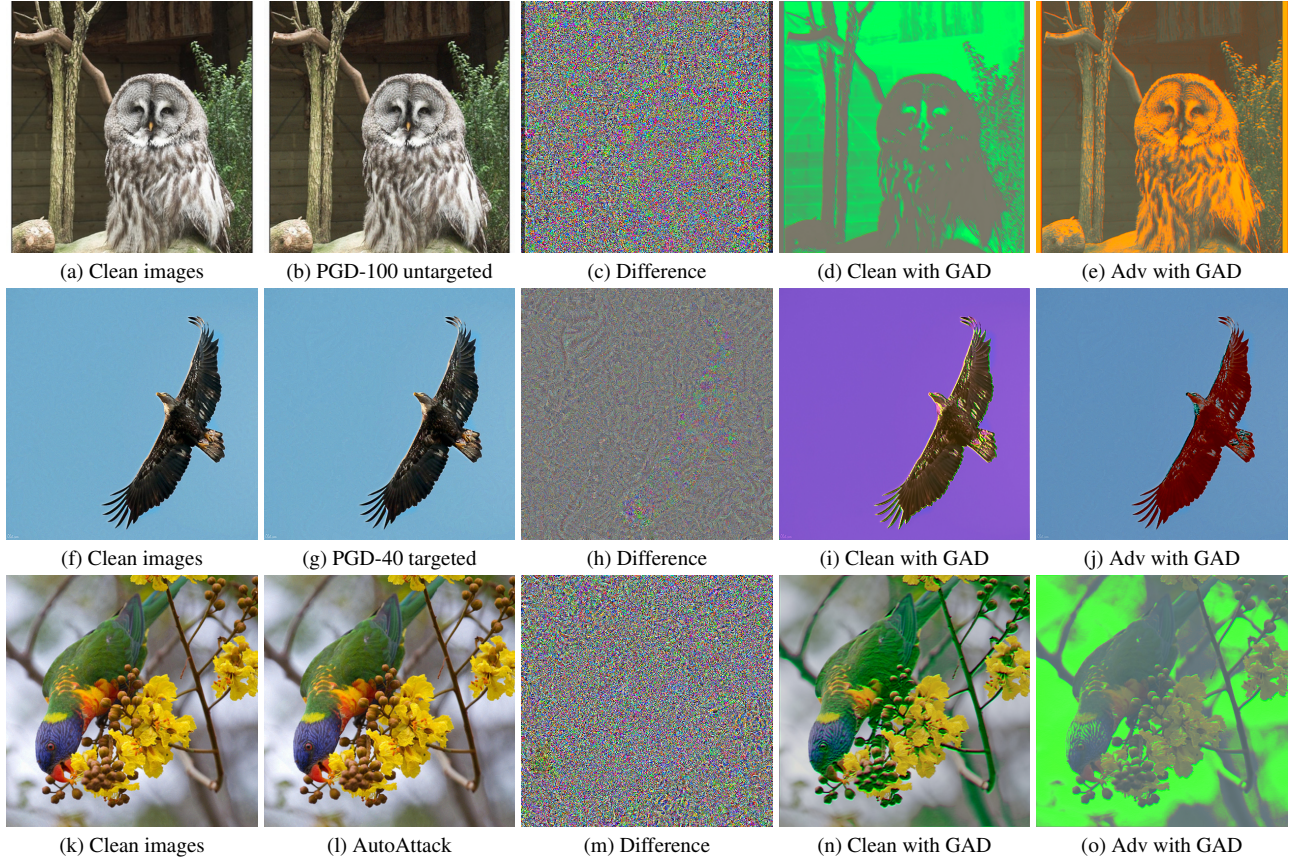


Figure 4. Examples of clean images, adversarial images, their differences, and the corresponding clean and adversarial images after applying GAD under three different attack settings.

Table 2. Comparison of individual GIR or SDF modules.

module	untargeted	targeted	AutoAttack
GAD	79.23/75.67	80.00/77.53	83.18/80.12
SDF	78.80/ 77.11	80.02/ 79.44	82.20/80.30
Combination	79.47 /76.43	80.73 /79.02	84.06 / 81.64

izer that prevents overfitting to adversarial noise without destroying useful semantic information, confirming that GAD and SDF capture complementary robustness properties.

Effect of shape encoding methods. We compare the proposed SDF with three alternative shape encodings: edges, contours, and skeletons, as in Tab. 3. For edge encoding, we employ the Canny operator to extract object boundaries. Contour extraction identifies continuous boundary curves by scanning the binary image for foreground-background transitions and grouping connected edge pixels into closed paths, thereby providing a detailed delineation of object geometry. Skeletonization iteratively prunes boundary pixels while preserving object connectivity, producing a one-pixel-wide medial axis that encodes the topological and

structural core of the shape. As illustrated in Fig. 5, each method captures distinct structural aspects of the object. Specifically, edges highlight sharp intensity transitions, contours outline the external silhouette, and the skeleton simplifies geometry to its essential topology. In contrast, the SDF encodes dense distance information where pixel intensity represents proximity to the object boundary. Quantitative results in Tab. 3 indicate that while all geometric representations enhance robustness, the SDF achieves the highest performance gains. This superior efficacy stems from the capacity of the SDF to capture continuous and discriminative shape information that is more resilient to adversarial noise compared to sparse or binary geometric descriptors.

Effect of GAD architectures. The GAD module employs a two layer convolutional network as the default backbone, where the initial layer produces two feature channels. To evaluate how architectural variations influence the effectiveness of appearance debiasing, we examine several alternative configurations as detailed in Tab. 4. The first variant is a two-layer residual architecture (*ResNet-2*), which utilizes three output channels in the first layer to enable residual

Table 3. Different shape information. Clean/Robust accuracy (%)

Shapes	untargeted	targeted	AutoAttack
Edge	75.76/72.26	80.43/78.59	82.32/79.39
Contour	76.10/73.07	80.76/78.83	82.47/79.48
Skeleton	75.79/72.32	80.31/78.31	82.41/80.49
SDF	79.47/76.43	80.73/79.02	84.06/81.64

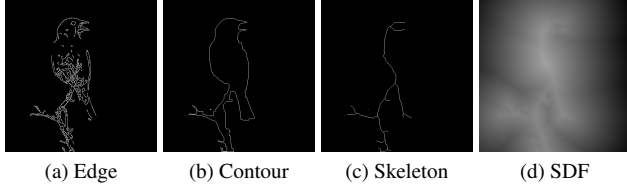


Figure 5. Visualization of diverse shape encodings, highlighting the unique geometric and structural characteristics of each method.

Table 4. Comparison of shallow networks used in the GAD module. The format is Clean/Robust accuracy (%).

GAD	untargeted	targeted	AutoAttack
ResNet-2	75.90/73.22	80.12/78.88	82.49/80.13
Attention	77.19/74.42	80.06/78.56	82.35/79.88
Linear	74.72/72.74	79.77/78.93	82.11/80.51
Convolution	79.47/76.43	80.73/79.02	84.06/81.64

addition. The second configuration explores an attention-based design that replaces standard convolutions with pixel-wise self-attention. In this setup, the queries (q), keys (k), and values (v) are derived from the input image, and the attention mechanism is computed as $\text{Softmax}(q \cdot k) \cdot v$ to preserve the original spatial resolution. The third variant consists of a two-layer linear network where projections are applied to transposed spatial dimensions to introduce appearance perturbations across both height and width. To ensure a fair comparison, Frobenius normalization is applied to the output of every configuration to maintain consistent energy scaling. The experimental results indicate that while all network variants achieve effective appearance debiasing, the convolutional configuration yields the most consistent and superior classification performance across all benchmarks.

Effect of classifiers. To demonstrate the architectural generality of ShapePuri, we evaluate the framework across multiple classifiers, including ResNet variants [7] (50, 101, and 152), ConvNeXt-L [13], and Swin-B [12]. The results in Tab. 5 indicate that all architectures achieve strong adversarial robustness when integrated with our framework. Specifically, ShapePuri achieves 80.59% (Swin-B model) and 81.36% (ConvNeXt-L model) robust accuracy under targeted attack, exhibiting higher performance gains when applied to larger-capacity networks.

Table 5. Different training models. Clean/Robust accuracy (%)

Train Models	untargeted	targeted	AutoAttack
ResNet-50	76.59/73.89	77.38/75.41	77.03/73.68
ResNet-101	79.47/76.43	80.19/77.94	79.69/76.28
ResNet-152	77.75/74.37	80.73/79.02	79.38/75.93
ConvNeXt-L	78.98/75.60	82.87/81.36	84.06/81.64
Swin-B	78.98/76.01	82.50/80.59	80.90/77.68

Table 6. Different attack models. Clean/Robust accuracy (%)

Attack model	untargeted	targeted	AutoAttack
ResNet-50	79.47/78.85	80.73/80.33	84.06/83.55
ResNet-101	79.47/76.43	80.73/80.28	84.06/83.38
ResNet-152	79.47/78.21	80.73/79.02	84.06/83.26
ConvNeXt-L	79.47/78.30	80.73/80.31	84.06/81.64

Effect of attack models. We examine the resilience of ShapePuri against adversarial perturbations generated by various attacker architectures to evaluate cross-architecture robustness, as shown in Tab. 6. The results demonstrate that large capacity classifiers exhibit superior resistance to attacks generated by smaller models. For instance, when a ConvNeXt-L model trained under the AutoAttack setting is evaluated against perturbations generated by ResNet-50, the robust accuracy reaches 83.55%, which nearly matches the clean accuracy of 84.06%. To ensure a rigorous and conservative assessment of robustness, we maintain identical architectures for both training and attacking models as the default setting for all experiments.

5. Conclusion

This paper introduces ShapePuri, a novel training framework designed to improve adversarial robustness by prioritizing geometric structure and mitigating unreliable appearance biases. The proposed approach reconciles two core modules through a multi stream supervision strategy: the Shape Encoding Module, which leverages Signed Distance Functions to reinforce structural awareness, and the Global Appearance Debiasing module, which uses stochastic convolutional layers to decorrelates predictions from non-robust textures. This unified training scheme allows the framework to internalize robust priors within the classifier parameters, enabling efficient inference without auxiliary computational overhead. Comprehensive evaluations demonstrate the efficacy of ShapePuri, which achieves 81.64% robust accuracy under the AutoAttack protocol. This performance establishes the first defense framework to exceed the 80% threshold while providing a scalable and robust paradigm for adversarial defense through the balance of structural fidelity and appearance debiasing.

Acknowledgments: High-performance computing resources were provided by the Erlangen National High Performance Computing Center (NHR@FAU) at Friedrich-Alexander-Universität Erlangen-Nürnberg (FAU), under the NHR projects b143dc and b180dc. NHR is funded by federal and Bavarian state authorities, and NHR@FAU hardware is partially funded by the German Research Foundation (DFG) – 440719683. Additional support was received by the ERC - project MIA-NORMAL 101083647, DFG 513220538, 512819079, and by the state of Bavaria (HTA).

References

- [1] Sajjad Amini, Mohammadreza Teymoorianfard, Shiqing Ma, and Amir Houmansadr. Meansparse: Post-training robustness enhancement through mean-centered feature sparsification. *CoRR*, 2024. [2](#), [6](#)
- [2] Mingyuan Bai, Wei Huang, Tenghui Li, Andong Wang, Junbin Gao, Cesar F Caiafa, and Qibin Zhao. Diffusion models demand contrastive guidance for adversarial purification to advance. In *Forty-first International Conference on Machine Learning (ICML)*, 2024. [2](#)
- [3] Louis Béthune, Paul Novello, Guillaume Coiffier, Thibaut Boissin, Mathieu Serrurier, Quentin Vincenot, and Andres Troya-Galvis. Robust one-class classification with signed distance function using 1-Lipschitz neural networks. In *Proceedings of the 40th International Conference on Machine Learning (ICML)*, pages 2245–2271. PMLR, 2023. [2](#)
- [4] Francesco Croce and Matthias Hein. Reliable evaluation of adversarial robustness with an ensemble of diverse parameter-free attacks. In *International conference on machine learning*, pages 2206–2216. ICML, 2020. [2](#), [6](#)
- [5] Robert Geirhos, Patricia Rubisch, Claudio Michaelis, Matthias Bethge, Felix A. Wichmann, and Wieland Brendel. Imagenet-trained CNNs are biased towards texture; increasing shape bias improves accuracy and robustness. In *International Conference on Learning Representations (ICLR)*, 2019. [2](#)
- [6] Sven Gowal, Sylvestre-Alvise Rebuffi, Olivia Wiles, Florian Stimberg, Dan Andrei Calian, and Timothy A Mann. Improving robustness using generated data. *Advances in neural information processing systems*, 34:4218–4233, 2021. [2](#)
- [7] Kaiming He, Xiangyu Zhang, Shaoqing Ren, and Jian Sun. Deep residual learning for image recognition. In *Proceedings of the IEEE Conference on Computer Vision and Pattern Recognition (CVPR)*, pages 770–778, 2016. [8](#)
- [8] Andrew Ilyas, Shibani Santurkar, Dimitris Tsipras, Logan Engstrom, Brandon Tran, and Aleksander Madry. Adversarial examples are not bugs, they are features. In *Advances in Neural Information Processing Systems (NeurIPS)*, 2019. [2](#)
- [9] Philip T. Jackson, Amir Atapour-Abarghouei, Stephen Bonner, Toby P. Breckon, and Boguslaw Obara. Style augmentation: Data augmentation via style randomization. In *Proceedings of the IEEE/CVF Conference on Computer Vision and Pattern Recognition (CVPR) Workshops*, pages 83–92, 2019. [2](#)
- [10] Chun Pong Lau, Jiang Liu, Hossein Souri, Wei-An Lin, Soheil Feizi, and Rama Chellappa. Interpolated joint space adversarial training for robust and generalizable defenses. *IEEE Transactions on Pattern Analysis and Machine Intelligence*, 45(11):13054–13067, 2023. [2](#)
- [11] Chun Tong Lei, Hon Ming Yam, Zhongliang Guo, Yifei Qian, and Chun Pong Lau. Instant adversarial purification with adversarial consistency distillation. In *Proceedings of the Computer Vision and Pattern Recognition Conference (CVPR)*, pages 24331–24340, 2025. [1](#), [2](#), [5](#), [6](#)
- [12] Ze Liu, Yutong Lin, Yue Cao, Han Hu, Yixuan Wei, Zheng Zhang, Stephen Lin, and Baining Guo. Swin transformer: Hierarchical vision transformer using shifted windows. In *Proceedings of the IEEE/CVF International Conference on Computer Vision (ICCV)*, pages 10012–10022, 2021. [8](#)
- [13] Zhuang Liu, Hanzi Mao, Chao-Yuan Wu, Christoph Feichtenhofer, Trevor Darrell, and Saining Xie. A convnet for the 2020s. In *Proceedings of the IEEE/CVF Conference on Computer Vision and Pattern Recognition (CVPR)*, pages 11976–11986, 2022. [8](#)
- [14] Aleksander Madry, Aleksandar Makelov, Ludwig Schmidt, Dimitris Tsipras, and Adrian Vladu. Towards deep learning models resistant to adversarial attacks. *The International Conference on Learning Representations (ICLR)*, 2018. [2](#), [6](#)
- [15] Weili Nie, Brandon Guo, Yujia Huang, Chaowei Xiao, Arash Vahdat, and Anima Anandkumar. Diffusion models for adversarial purification. *arXiv preprint arXiv:2205.07460*, 2022. [1](#), [2](#), [6](#)
- [16] Stanley Osher and James A Sethian. Fronts propagating with curvature-dependent speed: Algorithms based on hamilton-jacobi formulations. *Journal of Computational Physics*, 79(1):12–49, 1988. [3](#)
- [17] Cheng Ouyang, Chen Chen, Surui Li, Zeju Li, Chen Qin, Wenjia Bai, and Daniel Rueckert. Causality-inspired single-source domain generalization for medical image segmentation. *IEEE Transactions on Medical Imaging*, 42(4):1095–1106, 2022. [2](#), [5](#)
- [18] Jeong Joon Park, Peter Florence, Julian Straub, Richard Newcombe, and Steven Lovegrove. Deepsdf: Learning continuous signed distance functions for shape representation. In *Proceedings of the IEEE/CVF Conference on Computer Vision and Pattern Recognition (CVPR)*, pages 165–174, 2019. [2](#)
- [19] Pouya Samangouei, Maya Kabkab, and Rama Chellappa. Defense-gan: Protecting classifiers against adversarial attacks using generative models. *arXiv preprint arXiv:1805.06605*, 2018. [2](#)
- [20] Lukas Schott, Jonas Rauber, Matthias Bethge, and Wieland Brendel. Towards the first adversarially robust neural network model on MNIST. In *International Conference on Learning Representations (ICLR)*, 2019. [2](#)
- [21] Naman Deep Singh, Francesco Croce, and Matthias Hein. Revisiting adversarial training for imagenet: Architectures, training and generalization across threat models. *Advances in Neural Information Processing Systems*, 36:13931–13955, 2023. [2](#), [6](#)
- [22] Jinyi Wang, Zhaoyang Lyu, Dahua Lin, Bo Dai, and Hongfei

Fu. Guided diffusion model for adversarial purification.
arXiv preprint arXiv:2205.14969, 2022. [1](#), [2](#), [6](#)